

Tensorizing Flows: A Tool for Variational Inference

YUEHAW KHOO*, MICHAEL LINDSEY†, AND HONGLI ZHAO‡

Abstract. Fueled by the expressive power of deep neural networks, normalizing flows have achieved spectacular success in generative modeling, or learning to draw new samples from a distribution given a finite dataset of training samples. Normalizing flows have also been applied successfully to variational inference, wherein one attempts to learn a sampler based on an expression for the log-likelihood or energy function of the distribution, rather than on data. In variational inference, the unimodality of the reference Gaussian distribution used within the normalizing flow can cause difficulties in learning multimodal distributions. We introduce an extension of normalizing flows in which the Gaussian reference is replaced with a reference distribution that is constructed via a tensor network, specifically a matrix product state or tensor train. We show that by combining flows with tensor networks on difficult variational inference tasks, we can improve on the results obtained by using either tool without the other.

Key words. Variational inference, high-dimensional approximations, normalizing flows, tensor-train, matrix product state

AMS subject classifications. 68T07, 15A69, 62Dxx

1. Introduction. Normalizing flows [63, 62] define a category of probability distributions from which independent samples can be drawn directly. The deployment of neural network parametrizations [54] has supercharged the practical expressivity of normalizing flows, yielding noteworthy successes in generative modeling, i.e., the task of learning to sample from a distribution given limited examples. Normalizing flows are based on the idea of transforming a Gaussian base distribution via a sequence of invertible mappings, and this basic concept has been realized through an increasingly diverse array of architectures [15, 16, 36, 7]. For a recent review of normalizing flows and their myriad applications, see [53].

Among the other key paradigms for modern generative modeling, notably generative adversarial networks (GANs) [23] and variational autoencoders [38], normalizing flows are distinguished by the fact that the samples from the model come equipped with exact sample densities. This feature enables the direct application of normalizing flows to variational inference, e.g., in [49, 1], where one seeks to learn to sample from or compute expectations with respect to a probability distribution whose density function $p(\mathbf{x})$ is known *a priori* (up to a normalization constant).

Variational inference (VI) [33, 4] has emerged in recent decades as an alternative to Markov chain Monte Carlo (MCMC) methods [59], which can be confounded by long autocorrelation times despite in-principle exactness. In spite of the contrast, VI can be combined effectively with MCMC, as in [20, 2]. VI has found diverse applications from image processing and generation [37, 68], to reinforcement learning [18], to condensed matter physics [43, 64], and beyond.

VI starts with a parametric family $\{p_{\theta}\}$ of probability densities and seeks the best approximation of the target density p lying within this family by minimizing the

*Department of Statistics, University of Chicago, Illinois, IL 60637, USA. Email: ykhoo@uchicago.edu

†Department of Mathematics, University of California, Berkeley, Berkeley, CA 94720, USA. Email: lindsey@math.berkeley.edu

‡Committee on Computational and Applied Mathematics, University of Chicago, Illinois, IL 60637, USA. Email: honglizhaobob@uchicago.edu

Kullback-Leibler (KL) divergence

$$D_{\text{KL}}(p_{\theta}||p) = \int \log \left(\frac{p_{\theta}(\mathbf{x})}{p(\mathbf{x})} \right) p_{\theta}(\mathbf{x}) \, \mathbf{d}\mathbf{x}$$

over the low-dimensional vector of variational parameters θ . One major difficulty of VI is designing parametric classes of probability distributions that are sufficiently expressive while still permitting exact sampling with efficient density evaluation. Outside of normalizing flows, traditional approaches to VI have included parametrization via mixture models [22], inference networks [47], and implicit VI [65]. In flow-based approaches to VI, p_{θ} is parametrized as the pushforward of a base Gaussian distribution p_0 by a map T_{θ} which permits efficient inversion and Jacobian computation.

The other key difficulty of VI is optimizing the model parameters themselves, especially in the case where the target distribution p is multimodal. In the most extreme scenario, if the target is multimodal with well-separated modes and one’s current variational guess p_{θ} captures just a single modal component accurately, local optimization of the variational parameters cannot see the missing modes, and they are never successfully learned. In applications of normalizing flows to VI, the unimodality of the Gaussian reference p_0 results in a tendency toward “mode collapse” during parameter optimization, wherein only a single mode is learned accurately and others remain undiscovered. Even if the reference could be chosen, e.g., as a mixture of Gaussians, there is no guarantee that all modes will be discovered without any *a priori* knowledge about the modal structure. See [19] for an overview of these difficulties.

In principle, this problem would be cured if it were possible to instead optimize the KL divergence with the roles of p_{θ} and p exchanged, i.e., $D_{\text{KL}}(p||p_{\theta})$, which is in fact the objective used in generative modeling [54]. However, to train this objective, one must be able to sample from p , which is precisely the task that we are trying to accomplish in the first place. In [19, 2], schemes are proposed that use MCMC to adaptively sample from an increasingly accurate approximation for p as p_{θ} is trained. However, although such approaches can avoid mode collapse, they cannot fundamentally extend the capacity of the training to discover new modes (except those that can be discovered by reasonably long MCMC exploration).

More fundamentally, all uses of normalizing flows rely heavily on the expressive power of neural networks to correct the base distribution p_0 . If p is far from Gaussian, even if an approximation $p_{\theta} \approx p$ can be effectively learned, a good approximation may require a neural network parametrization that is expensive to train.

Therefore, there is ample motivation to construct a reference p_0 that approximates the global structure of p . If this can be accomplished, one might bypass difficulties imposed by multimodality and moreover, get away with more compact and easily trainable neural network parametrizations of the flow map. Several works have considered improvements of the base distribution. For capturing heavy-tailed distributions, [31] has considered the use of density quantile function, whereas [44] proposes to use copulas as base distributions. Meanwhile, [60] adaptively exploits accept-reject re-sampling. However, none of these approaches can incorporate *a priori* knowledge about the global modal structure of the target distribution.

Tensor networks originally emerged from the numerical study of quantum many-body problems. They provide low-dimensional parametrizations capable of overcoming the curse of dimensionality that prevents many-particle wavefunctions from being stored exactly. The most widely used and successful tensor network remains the matrix product state (MPS), which emerges in tandem with the density matrix renormalization group (DMRG) algorithm for computing many-body ground states [67].

The same structure has also appeared as the tensor train (TT) [52] in the applied mathematics literature, where it is often viewed within the broader context of generalizing the singular value decomposition to higher-order tensors [42, 14]. In recent years, low-rank tensor decompositions have received increasing attention, for example, in surrogate modeling and deep learning [50, 8, 61]. Among many formats, the TT format is distinguished by the ease with which it allows for various key operations to be performed, with complexity that depends only linearly on the problem dimension, as long as the core tensor ranks remain bounded. Moreover, various TT operations also support convenient parallelism [56, 13]. Many high-dimensional classical problems, such as generative modeling [29], variational Bayes inference [69, 25], supervised learning [12], numerical partial differential equations [34, 55], and dynamical systems [40] can in important instances be recast and solved efficiently in the TT format.

In a VI setting, one is given (up to normalization) the density $p(\mathbf{x})$ as a black-box function. Therefore, cross-approximation can be applied to obtain the components of a TT. In this work, we propose to combine the advantages of NF and TT for the purpose of VI. We construct a base TT distribution by squaring a functional tensor train [58] obtained from a cross approximation [51] of the square root of the target density [48]. Relative to [17], this ensures the non-negativity and exact sample-ability of the base distribution. Then we push forward our base distribution by a flow map parametrized with neural networks. We refer to our model as a *tensorizing flow* (TF) since the advantages of both tensor decompositions and flow-based models are combined. Like NF, TF admits exact sampling equipped with sample densities. However, it demonstrates improved performance over straightforward NFs at comparable computational cost, measured in terms of the variational objective. Meanwhile, the flow is able to improve the base TT distribution obtained directly with numerical linear algebra routines. We demonstrate the advantage of our method on a Ginzburg-Landau model [26, 45] that we find to be intractable to approach with either NF or TT individually, as well as other high-dimensional test distributions of interest.

Our contribution: In this paper, we tackle the problem of initializing the base distribution for a normalizing flow. This is achieved with tensor network methods, which ultimately reduce to fast linear algebra routines. In particular, we leverage tensor-train orthogonalizations to improve the linear scaling in the recently proposed squared inverse Rosenblatt transport [10] method for interpolating probability densities with guaranteed non-negativity. From another perspective, our method can be viewed as an improvement over TT-based generative model [11], by augmenting it with a neural-network flow model, as TT has a limited representation power.

1.1. Organization. We review the background materials on VI and NF in Section 2. In Section 3 we detail the methodology for constructing the base distribution using a squared TT representation and for generating samples (equipped with densities) at computational cost scaling linearly with dimension for fixed ranks. The final TF model is tested on a variety of high-dimensional probability distributions in Section 4.

1.2. Notation. For a positive integer $n \in \mathbb{N}$, throughout we denote $[n] := \{1, 2, \dots, n\}$. Throughout the text, d shall denote the problem dimension, i.e., the dimension of the sampling variable \mathbf{x} . Given $n_1, \dots, n_k \in \mathbb{N}$ and indices $i_j \in [n_j]$, $1 \leq j \leq k$, we will often consider multi-indices of the form $\mathcal{I} := (i_1, \dots, i_k)$. We use square brackets to represent discretely indexed tensor values, e.g., $\mathcal{A}[\mathcal{I}]$ for a suitable d -tensor \mathcal{A} . Meanwhile we use parentheses to denote continuous function evaluations, e.g., $p(\mathbf{x})$. To describe sub-tensors of a tensor, we adopt the widely-used ‘MATLAB

notation.’ For instance, if $\mathbf{A} \in \mathbb{R}^{m \times n}$ denotes a matrix or 2-tensor, then $\mathbf{A}[i, j]$ represents a single element, while $\mathbf{A}[i, :]$ and $\mathbf{A}[:, j]$ represent the i -th row and j -th column, respectively. In naming objects, we will use non-boldface lowercase letters to denote scalars (e.g., $a, u, v \in \mathbb{R}$), boldface lowercase letters for vectors (e.g., $\mathbf{v}, \mathbf{w} \in \mathbb{R}^n$), boldface uppercase letters for matrices (e.g., $\mathbf{A}, \mathbf{B} \in \mathbb{R}^{m \times n}$), and calligraphic uppercase letters for general high-dimensional tensors (e.g., $\mathcal{A}, \mathcal{C} \in \mathbb{R}^{n_1 \times \dots \times n_d}$). There may be exceptions to this rule as becomes necessary, but these will be explicitly noted.

Finally, several tensor network diagrams [5] are presented to better illustrate tensor train operations. In this work, a tensor diagram is composed of nodes and edges, where the nodes represent a ‘core tensors’ out of which a large tensor associated to the diagram is built. In general, we allow for tensors with mixed discrete and continuous indices by thinking of them simply as functions jointly of some discrete and some continuous variables. The number of outgoing edges from a node represents the order of the tensor, i.e., the number of indices. Connections between outgoing edges indicate that the corresponding indices are shared and summed (or integrated) out in the overall tensor, cf. Section 2.3, where we shall review other special notations as needed.

2. Background and preliminaries. We introduce the general variational inference problem in Section 2.1 along with its implementation using normalizing flows in Section 2.2. Section 2.3 reviews the matrix product state (MPS) / tensor train (TT) decomposition, summarizes necessary operations in this format, and discusses its application to efficient compression of high-dimensional probability distributions.

2.1. Variational inference. Given a function $U : \Omega \rightarrow \mathbb{R}$, we would like to learn a target density defined as:

$$p(\mathbf{x}) = \frac{1}{Z} e^{-U(\mathbf{x})}, \quad (2.1)$$

where $Z = \int_{\Omega} e^{-U(\mathbf{x})} d\mathbf{x}$ is the normalizing constant or partition function.

In variational inference (VI), one formulates the partition function in terms of the optimal value of an optimization problem. More precisely, given a family of distributions \mathcal{P} , one minimizes

$$\begin{aligned} L(\tilde{p}) &:= \mathbb{E}_{\mathbf{x} \sim \tilde{p}} \left[\log \tilde{p}(\mathbf{x}) + U(\mathbf{x}) \right] \\ &= D_{\text{KL}}(\tilde{p} || p) - \log Z. \end{aligned} \quad (2.2)$$

over $\tilde{p} \in \mathcal{P}$. Here D_{KL} denotes the Kullback-Leibler (KL) divergence.

Assuming that $p \in \mathcal{P}$, the optimal value of this minimization problem is $-\log Z$, which is attained if and only if $D_{\text{KL}}(\tilde{p} || p) = 0$, i.e., if and only if $\tilde{p} = p$. If $p \notin \mathcal{P}$, then optimizing (2.2) recovers the best approximation of p within the family \mathcal{P} , as measured by the KL divergence.

The expectation in (2.2) can be estimated using a finite set of samples $\{\mathbf{x}^{(s)}\}_{s=1}^S$ drawn from \tilde{p} , provided we can compute the densities $\tilde{p}(\mathbf{x}^{(s)})$ of our samples.

2.2. Variational inference with normalizing flows. In practical applications, we consider a family of distributions parametrized by $\boldsymbol{\theta}$. Denoting now the parametrized distribution as $p_{\boldsymbol{\theta}}$, we seek to solve:

$$\boldsymbol{\theta}^* = \underset{\boldsymbol{\theta}}{\operatorname{argmin}} L(\boldsymbol{\theta}),$$

where we now abuse notation slightly by identifying $L(\boldsymbol{\theta}) = L(p_{\boldsymbol{\theta}})$.

The accuracy of VI is ultimately limited by the expressivity of the parametrized family $\{p_{\boldsymbol{\theta}}\}$. In this work, we focus on families based on normalizing flows. More precisely, we construct $p_{\boldsymbol{\theta}}$ as the *pushforward* of a fixed base distribution p_0 by the composition of a sequence $F_{\boldsymbol{\theta}}^{(k)}$, $k = 1, \dots, K$, of differentiable invertible maps, as in

$$T_{\boldsymbol{\theta}} := F_{\boldsymbol{\theta}}^{(K)} \circ \dots \circ F_{\boldsymbol{\theta}}^{(1)},$$

which are themselves parametrized by a collection of neural network parameters $\boldsymbol{\theta}$. The number K of maps is the length of the flow. It is useful to denote

$$T_{\boldsymbol{\theta}}^{(k)} := F_{\boldsymbol{\theta}}^{(k)} \circ \dots \circ F_{\boldsymbol{\theta}}^{(1)},$$

with $T_{\boldsymbol{\theta}}^{(0)} := \text{Id}$, so $T_{\boldsymbol{\theta}}^{(k+1)} = F_{\boldsymbol{\theta}}^{(k+1)} \circ T_{\boldsymbol{\theta}}^{(k)}$ for $k = 0, \dots, K-1$, and $T_{\boldsymbol{\theta}}^{(K)} = T_{\boldsymbol{\theta}}$.

Concretely, to sample $\mathbf{x} \sim p_{\boldsymbol{\theta}}$, one samples $\mathbf{z} \sim p_0$ and computes $\mathbf{x} = T_{\boldsymbol{\theta}}(\mathbf{z})$. The model density of a sample \mathbf{x} can be computed by change of variables as

$$p_{\boldsymbol{\theta}}(\mathbf{x}) = p_0(T_{\boldsymbol{\theta}}^{-1}(\mathbf{x})) |DT_{\boldsymbol{\theta}}^{-1}(\mathbf{x})|.$$

Then observe that the loss can be written as an expectation with respect to the base distribution:

$$L(\boldsymbol{\theta}) = \mathbb{E}_{\mathbf{z} \sim p_0} \left[\log p_0(\mathbf{z}) - \log |DT_{\boldsymbol{\theta}}(\mathbf{z})| + U(T_{\boldsymbol{\theta}}(\mathbf{z})) \right],$$

which can be further unpacked as

$$L(\boldsymbol{\theta}) = \mathbb{E}_{\mathbf{z} \sim p_0} \left[\log p_0(\mathbf{z}) - \sum_{k=1}^K \log \left| DF_{\boldsymbol{\theta}}^{(k)} \left(T_{\boldsymbol{\theta}}^{(k-1)}(\mathbf{z}) \right) \right| + U(T_{\boldsymbol{\theta}}(\mathbf{z})) \right]. \quad (2.3)$$

By drawing S independent samples $\mathbf{z}^{(1)}, \dots, \mathbf{z}^{(S)} \sim p_0$, the loss (2.3) can be estimated empirically as

$$\widehat{L}(\boldsymbol{\theta}) = \frac{1}{S} \sum_{s=1}^S \left[\log p_0(\mathbf{z}^{(s)}) - \sum_{k=1}^K \log \left| DF_{\boldsymbol{\theta}}^{(k)} \left(T_{\boldsymbol{\theta}}^{(k-1)}(\mathbf{z}^{(s)}) \right) \right| + U(T_{\boldsymbol{\theta}}(\mathbf{z}^{(s)})) \right], \quad (2.4)$$

and the gradient $\nabla_{\boldsymbol{\theta}} L(\boldsymbol{\theta})$ can be estimated via the ‘reparametrization trick,’ i.e., by freezing the samples $\mathbf{z}^{(1)}, \dots, \mathbf{z}^{(S)}$ and automatically differentiating through the evaluation formula (2.4).

The sequence of mappings $F_{\boldsymbol{\theta}}^{(1)}, \dots, F_{\boldsymbol{\theta}}^{(K)}$ are chosen to balance expressivity with efficient computation of the determinant of the Jacobian. We refer the reader to [41] for a variety of choices. Some popular architectures include NICE [15], FFJORD [24], and RealNVP [16]. In this work we opt for invertible residual networks, or iResNets [3, 6].

2.3. Tensor operations. In this section, we summarize certain fundamental tensor operations.

We illustrate tensor contraction and the associated notation with illustrative examples. More formal definitions can be found, for example, in [39]. Tensor contraction is loosely defined as summation/integration over repeated indices/arguments. For instance, consider a 3-tensor $\mathcal{A} \in \mathbb{R}^{n_1 \times n_2 \times n_3}$ and a matrix $\mathbf{B} \in \mathbb{R}^{n_2 \times m_2}$. A new tensor

\mathcal{C} of size $n_1 \times m_2 \times n_3$ can be formed by contracting the middle index of \mathcal{A} with the first index of \mathbf{B} :

$$\mathcal{C}[i_1, j_2, i_3] = \sum_{k_2} \mathcal{A}[i_1, k_2, i_3] \mathbf{B}[k_2, j_2] =: \langle \mathcal{A}[i_1, k_2, i_3], \mathbf{B}[k_2, j_2] \rangle_{k_2 \in [n_2]} \quad (2.5)$$

One may consider a function to be a tensor by identifying indices with function arguments, and one can define suitable tensor contractions analogously. For example, letting $k : X_1 \times X_2 \rightarrow \mathbb{R}$ and $g : X_2 \rightarrow \mathbb{R}$, a new function $f : \mathbb{R} \rightarrow \mathbb{R}$ can be defined as:

$$f(x_1) = \int_{X_2} k(x_1, x_2) g(x_2) dx_2 = \langle k(x_1, x_2), g(x_2) \rangle_{x_2 \in X_2}. \quad (2.6)$$

One can also define a mixed-type contraction such as the following¹:

$$\mathcal{C}_{i_1 i_3}(x_2) := \mathcal{C}[i_1, x_2, i_3] = \sum_{i_2} \mathcal{C}[i_1, i_2, i_3] f_{i_2}(x_2) =: \langle \mathcal{C}[i_1, i_2, i_3], f_{i_2}(x_2) \rangle_{i_2 \in [n_2]} \quad (2.7)$$

In the above equations, we introduced the bracket notation as a shorthand to denote contractions over certain indices / continuous spaces. We will occasionally revisit this notation to render lengthy summations over multiple indices more readable.

In this work, special cases of contractions such as tensor-tensor, tensor-matrix and tensor-vector contractions are frequently encountered. Contractions can be used to combine low-order tensors into a high-order tensor. For instance, a tensor train constructs a d dimensional tensor from several 3-tensors.

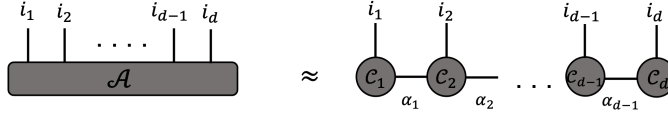


Fig. 2.1: Tensor-train decomposition of a d -dimensional tensor

DEFINITION 2.1. (*Tensor train decomposition*) A tensor $\mathcal{A} \in \mathbb{R}^{n_1 \times \dots \times n_d}$ is a tensor train (TT) with ranks (r_0, \dots, r_d) , where $r_0 = r_d = 1$, if it can be written

$$\begin{aligned} \mathcal{A}[\mathcal{I}] &= \sum_{\alpha_1=1}^{r_1} \dots \sum_{\alpha_{d-1}=1}^{r_{d-1}} \mathcal{C}_1[1, i_1, \alpha_1] \mathcal{C}_2[\alpha_1, i_2, \alpha_2] \dots \mathcal{C}_d[\alpha_{d-1}, i_d, 1] \\ &= \mathcal{C}_1[1, i_1, :] \mathcal{C}_2[:, i_2, :] \dots \mathcal{C}_d[:, i_d, 1], \end{aligned}$$

where $\mathcal{I} = (i_1, \dots, i_d)$, the last equality is simply a sequence of matrix multiplications, and the 3-tensors $\mathcal{C}_i \in \mathbb{R}^{r_{i-1} \times n_i \times r_i}$ are called the core tensors.

A tensor diagram illustration is presented in Figure 2.1, using conventions described in Section 1.2.

The advantage of this decomposition is that it allows us to store and compute with the list of cores $\{\mathcal{C}_i\}_{i=1}^d$, instead of the full tensor \mathcal{A} , which has $O(n^d)$ elements. If the ranks are low, the computational cost of various operations can be reduced

¹When there are mixed (i.e., both discrete and continuous) indices, we generally prefer to write the discrete indices as subscripts.

significantly. Indeed, storage scales as $O(dnr^2)$, and evaluation of a single entry of the tensor scales as $O(dr^2)$. Common arithmetic operations with TTs, such as addition, can be implemented within the TT format by manipulating the cores only, as summarized in [52]. The TT ranks can be truncated optimally via SVDs of unfolding matrices [52].

Finally, we introduce the orthogonalization operation on a TT, also known as canonicalization in the MPS literature. This procedure orthogonalizes each TT core in a sequential fashion until all but one core is orthogonalized. Using tensor diagram notation, we present the orthogonalized TT decomposition in Figure 2.2 and refer the interested reader to [52, 21] for more details. We mark the orthogonalized cores as half-solid to distinguish them from the original ones, as introduced in [27]. The light side of the node indicates that for orthogonalized cores \mathcal{Q}_k have orthonormal rows after suitable matricization, i.e., that

$$\langle \mathcal{Q}_k[:, i_k, \alpha_k], \mathcal{Q}_k[:, i_k, \alpha_k] \rangle_{i_k, \alpha_k} = I_{r_{k-1}}, \text{ for all } k = 2, \dots, d \quad (2.8)$$

The TT in Figure 2.2 is referred to as *right-left orthogonal*. The orthogonalization procedure costs $O(dnr^3)$ operations.

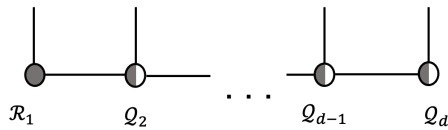


Fig. 2.2: Illustration of the TT right-left orthogonal form.

3. Proposed method. We present in this section the construction of the tensorizing flow. We consider a target distribution p of form (2.1) to be approximated on a domain $\Omega = [a_1, b_1] \times \dots \times [a_d, b_d] \subset \mathbb{R}^d$. By shifting and scaling the domain, we can always assume that $\Omega = [-1, 1]^d$. Within the flow framework of (2.3)-(2.4), rather than choosing a Gaussian base distribution p_0 , we will use a TT to construct a base distribution p_0 that already approximates the target p reasonably well. In order to optimize the empirical loss (2.4), we are required to be able to efficiently achieve the following with p_0 :

- draw samples $\mathbf{z} \sim p_0$.
- compute sample densities $p_0(\mathbf{z})$.

In Section 3.1, we will construct $p_0 \approx p$ using a TT in a way that meets these criteria. In Section 3.2, we will present our specific choice of flow maps $F_{\theta}^{(k)}$ based on invertible residual networks.

3.1. Base distribution. We will construct $p_0(\mathbf{x})$ as the pointwise square of a functional tensor train [10] denoted $q_0(\mathbf{x})$. In Section 3.1.1 we explain how samples equipped with densities can be drawn from such a p_0 , and in Section 3.1.4 we explain how q_0 can be prepared using only the ability to evaluate the energy function $U(\mathbf{x})$ defining the target $p(\mathbf{x}) \propto \exp(-U(\mathbf{x}))$.

3.1.1. Autoregressive sampling framework. Sampling from a multivariate distribution is in general a nontrivial task. In the style of other work using MPS/TT for generative modeling [9, 29, 48], we will draw a sample $\mathbf{x}^* \sim p_0$ ‘autoregressively,’

i.e., by writing:

$$p_0(x_1, \dots, x_d) = p_1(x_1)p_2(x_2|x_1) \cdots p_d(x_d|x_1, \dots, x_{d-1}), \quad (3.1)$$

then sampling each successive coordinate x_k^* from the appropriate conditional distribution, conditioned on previously sampled coordinates x_j , $j = 1, \dots, k-1$.

In other words, for each $k = 1, 2, \dots, d$, we would like to sample

$$x_k^* \sim p_k(x_k|\mathbf{x}_{<k}^*), \quad (3.2)$$

where $\mathbf{x}_{<k}^* = (x_1^*, x_2^*, \dots, x_{k-1}^*)$. This approach converts the problem of obtaining a multivariate sample $\mathbf{x}^* = (x_1^*, \dots, x_d^*)$ into sequence of univariate sampling problems, which we can view as essentially trivial. The difficulty is to construct these univariate distributions. By the definition of conditional probability:

$$p_k(x_k|\mathbf{x}_{<k}^*) = \frac{p_0(\mathbf{x}_{<k}^*, x_k)}{p_{<k}(\mathbf{x}_{<k}^*)} \propto p_{<k+1}(\mathbf{x}_{<k}^*, x_k), \quad (3.3)$$

viewing the previously sampled coordinates as fixed. Here we have defined the marginal distributions:

$$p_{<k}(\mathbf{x}_{<k}) := \int p_0(x_1, \dots, x_k, x_{k+1}, \dots, x_d) dx_{k+1} \dots dx_d \quad (3.4)$$

Therefore, to construct the univariate distributions that we need, we will essentially only need to marginalize p_0 , possibly with some leading variables fixed.

3.1.2. Representation of p_0 . To deal with the continuum in even a single component, we discretize by considering a truncated orthonormal basis ϕ_1, \dots, ϕ_n for $L^2([-1, 1])$, furnished by, e.g., orthogonal polynomials. In practice we can choose a different basis size n_j for each dimension $j = 1, \dots, d$, but for simplicity of the discussion we will just consider the case of uniform $n_j = n$.

For the time being, assume that we are also given a d -dimensional tensor train $\mathcal{C} \in \mathbb{R}^{n \times \dots \times n}$ that specifies the coefficients of a function

$$q_0(\mathbf{x}) \approx q(\mathbf{x}) := \sqrt{p(\mathbf{x})}$$

in the d -fold tensor product basis induced by $\{\phi_i\}_{i=1}^n$. Our approximate density, $p_0 \approx p$, can then be obtained as the pointwise square $p_0(\mathbf{x}) = q_0(\mathbf{x})^2$.

Concretely, suppose

$$q_0(\mathbf{x}) = \sum_{\mathcal{I}} \mathcal{C}[\mathcal{I}] \phi_{\mathcal{I}}(\mathbf{x}) = \sum_{i_1=1}^n \cdots \sum_{i_d=1}^n \mathcal{C}[i_1, \dots, i_d] \phi_{i_1}(x_1) \cdots \phi_{i_d}(x_d), \quad (3.5)$$

where the pure tensor product functions $\phi_{\mathcal{I}}$ and coefficient tensor $\mathcal{C}[\mathcal{I}]$ satisfy

$$\phi_{\mathcal{I}}(\mathbf{x}) := \phi_{i_1}(x_1) \cdots \phi_{i_d}(x_d), \quad \mathcal{C}[\mathcal{I}] = \langle q_0(\mathbf{x}), \phi_{\mathcal{I}}(\mathbf{x}) \rangle_{\mathbf{x} \in \Omega}.$$

Let the cores of \mathcal{C} be denoted $\mathcal{C}_1, \dots, \mathcal{C}_d$. The details of obtaining \mathcal{C} as a TT are deferred for now to Section 3.1.4.

We remark here that although we intend to obtain samples from $p_0(\mathbf{x}) = q_0(\mathbf{x})^2$, we never explicitly form its coefficient tensor as a TT, as doing so would require us to work with core tensors of size $r^2 \times n \times r^2$ [11]. Instead we only work directly with

the core tensors of \mathcal{C} . In particular, we demonstrate that by putting the cores of \mathcal{C} in right-left orthogonal form, the marginalizations in variables x_{k+1}, \dots, x_d required in the sampling process (3.2) can be performed for free, and the entire cost of drawing a sample will scale only linearly with the dimension d .

As such, before discussing further details, we define a right-left orthogonalization of \mathcal{C} ,

$$\mathcal{C}[i_1, \dots, i_d] = \mathcal{R}_1[1, i_1, :] \mathcal{Q}_2[:, i_2, :] \cdots \mathcal{Q}_d[:, i_d, 1],$$

which can be computed in $O(dnr^3)$ time as reviewed in Section 2.3. See Figure 2.2 for a diagram.

3.1.3. Sampling algorithm. Now we discuss how to produce exact samples $\mathbf{x}^* \sim p_0$ given \mathcal{C} as a TT in right-left orthogonal form. At any step $k = 1, \dots, d$, we need to have a representation of the marginal

$$p_{<k+1}(\mathbf{x}_{<k}^*, x_k) = \int q_0(x_1^*, \dots, x_{k-1}^*, x_k, \dots, x_d)^2 dx_{k+1} \cdots dx_d \quad (3.6)$$

in order to generate a coordinate sample x_k^* . The function $q_0(\mathbf{x})$ can be represented with a tensor network diagram with continuous external legs by attaching the mixed tensors $\phi_i(x)$ to the external legs of the TT diagram for \mathcal{C} , as depicted in Figure 3.1.

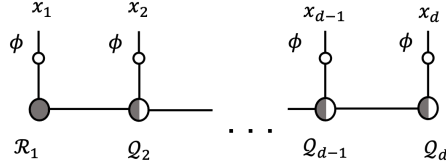


Fig. 3.1: Illustration of $q_0(\mathbf{x})$ as a tensor network, composed of a tensor train coefficient \mathcal{C} with continuous univariate functions $\phi_i(x_i)$ in each dimension. It can be interpreted as a mixed-type tensor with both discrete and continuous indices.

The tensor contractions required to compute (3.6) are depicted in Figure 3.2. Orthonormality of the univariate basis functions ϕ_1, \dots, ϕ_n guarantees that the integration in (3.6) yields identity matrices forming the rungs of a ‘ladder’ to the right of the k -th cores in Figure 3.2(a). Meanwhile, fixing the previous coordinates x_1^*, \dots, x_{k-1}^* amounts to computing tensor-vector contractions between the cores $\mathcal{R}_1, \mathcal{Q}_2, \dots, \mathcal{Q}_{k-1}$ and vectors $\phi_1^*, \phi_2^*, \dots, \phi_{k-1}^*$ of basis function evaluations, defined by

$$\phi_j^* = \begin{bmatrix} \phi_1(x_j^*) \\ \vdots \\ \phi_n(x_j^*) \end{bmatrix} \in \mathbb{R}^n, \quad (3.7)$$

as depicted in Figure 3.2(a). There we denote the matrices resulting from these tensor-vector contractions as $\mathbf{R}_1^*, \mathbf{Q}_2^*, \dots, \mathbf{Q}_{k-1}^*$, respectively.

In passing from frame (a) to frame (b) of Figure 3.2, right-left orthogonality allows us to simply ‘collapse the ladder’ from right to left in the tensor network diagram without any additional computation. To pass from frame (b) to frame (c), the left tail of the train can be collapsed into a single vector \mathbf{v}_{k-1} by the indicated

sequence of matrix-vector multiplications. To maintain linear dimension scaling, the computation of \mathbf{v}_{k-2} can simply be recycled from the preceding step, and \mathbf{v}_{k-1} can be produced with only a single additional matrix multiplication.

In frame (c), the core $\mathbf{Q}_k \in \mathbb{R}^{r_{k-1} \times n \times r_k}$ is contracted with $\mathbf{v}_{k-1} \in \mathbb{R}^{r_{k-1}}$ to produce a matrix $\mathbf{B}_k \in \mathbb{R}^{n \times r_k}$. In passing from frame (c) to frame (d), we perform the matrix-matrix multiplication defining $\mathbf{A}_k := \mathbf{B}_k \mathbf{B}_k^\top$, and from frame (d) it is clear that

$$f_k(x_k) := p_{<k+1}(\mathbf{x}_{<k}^*, x_k) = \sum_{i,j=1}^n \mathbf{A}_k[i,j] \phi_i(x_k) \phi_j(x_k). \quad (3.8)$$

Note that \mathbf{A}_k is positive semidefinite by construction, guaranteeing pointwise non-negativity of this expression as a function of x_k .

Now following (3.3), we know that the univariate function f_k is proportional to the univariate conditional probability density $p_k(x_k | \mathbf{x}_{<k}^*)$ from which we wish to draw a sample. If the ϕ_1, \dots, ϕ_n are polynomials such as Legendre or Chebyshev polynomials, the CDF can be computed exactly and then a sample can be drawn using the inverse CDF method through efficient root-finding. In practice, it is also efficient to just evaluate f_k on a finely spaced grid and implement the inverse CDF method via the trapezoidal rule.

Given a multivariate sample $\mathbf{x}^* = (x_1^*, \dots, x_d^*)$ furnished by our sampling routine, it is trivial to recover its density $p_0(\mathbf{x}^*)$. Indeed, observe based on the definition (3.8) that $f_d(x_d^*) = p_0(\mathbf{x}^*)$, so we need only evaluate the final univariate function f_d that we have constructed at the final coordinate sample x_d^* .

In summary, once \mathcal{C} has been furnished as a TT, the entire cost of producing N samples from p_0 scales as

$$O(dnr^3 + Ndn^2r^2),$$

Here the first term is associated to the right-left orthogonalization pre-processing step, and we have defined $r := \max_{i=1, \dots, d-1} \{r_i\}$ as the maximal TT rank of \mathcal{C} . Recall moreover that n is the size of the univariate basis ϕ_1, \dots, ϕ_n , and d is the problem dimension.

3.1.4. Obtaining \mathcal{C} as a TT. It remains to discuss how to produce the coefficient tensor \mathcal{C} of $q_0(\mathbf{x})$ in TT format. The key difficulty of this section is to figure out how to leverage the TT-cross algorithm [51].

Recall from (2.1) that $p \propto \tilde{p} := e^{-U}$, where we have defined \tilde{p} to be an unnormalized density that we are capable of evaluating pointwise. Recall further that we want a TT-based approximation q_0 of $q = \sqrt{p}$. First we will obtain a TT-based approximation \tilde{q}_0 of $\tilde{q} := \sqrt{\tilde{p}}$, and then we will recover an appropriate q_0 via a normalization step.

We will also express \tilde{q}_0 in terms of a coefficient tensor, namely \mathcal{B} , with respect to our functional tensor product basis:

$$\tilde{q}_0(\mathbf{x}) = \sum_{\mathcal{I}} \mathcal{B}[\mathcal{I}] \phi_{\mathcal{I}}(\mathbf{x}). \quad (3.9)$$

The coefficient tensor \mathcal{B} will differ from the coefficient tensor \mathcal{C} that we seek by only a scalar constant factor that we will compute later.

TT-cross is most naturally suited to recovering a function defined on a multivariate grid, which can be viewed as an ordinary tensor with discrete indices. As such we

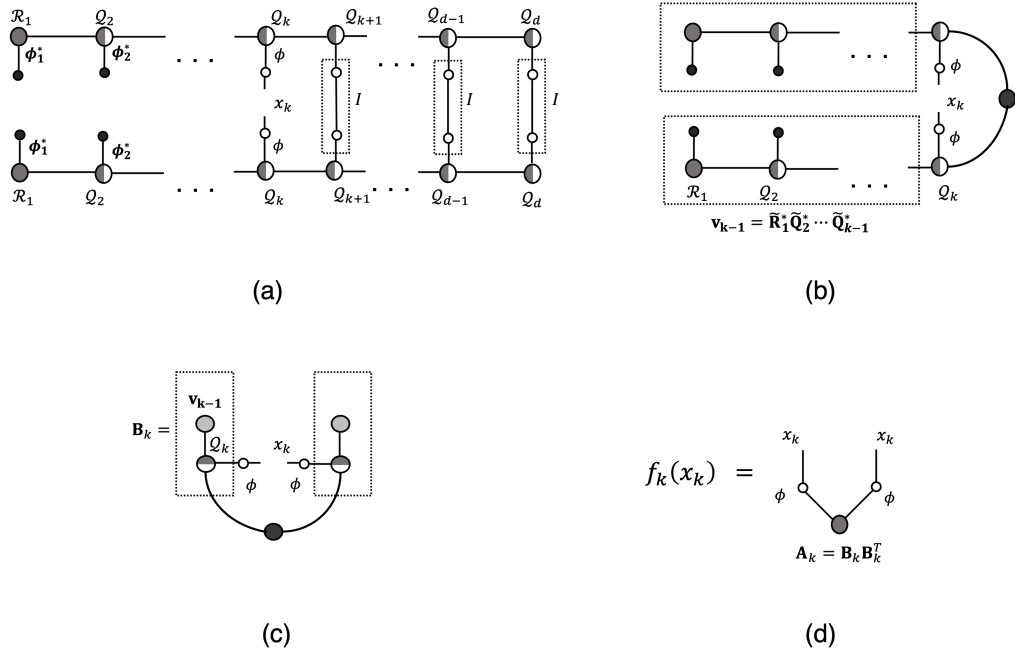


Fig. 3.2: Construction of $f_k(x_k) := p_{<k+1}(\mathbf{x}_{<k}^*, x_k)$. For a detailed step-by-step description of the procedure, refer to the main text of Section 3.1.3.

will use TT-cross to recover a TT-based approximation of \tilde{q} on such a grid and then use numerical quadrature to deduce an appropriate coefficient tensor \mathcal{B} .

To this end, let $x^{(1)}, \dots, x^{(m)} \in [-1, 1]$ denote univariate quadrature points, with associated quadrature weights $w^{(1)}, \dots, w^{(m)} \in \mathbb{R}$. As we commented for the univariate basis functions $\phi_1, \dots, \phi_n \in L^2([-1, 1])$, it is possible to choose a different set of quadrature points $x_k^{(1)}, \dots, x_k^{(m_k)}$ (and weights) for each dimension $k = 1, \dots, d$, but for simplicity we simply adopt the same choice for each dimension and in particular $m_k = m$ for all $k = 1, \dots, d$.

To avoid confusion with the multi-index notation \mathcal{I} that we use to denote basis coefficients, we will use $\mathcal{J} = (j_1, \dots, j_d)$ to index the multivariate grid, defining the tensor $\mathcal{T} \in \mathbb{R}^{m \times \dots \times m}$ of grid values for \tilde{q} by

$$\mathcal{T}[\mathcal{J}] := \tilde{q}(x^{(j_1)}, \dots, x^{(j_d)}). \quad (3.10)$$

Now TT-cross can be applied precisely to determine a TT approximation $\mathcal{S} \approx \mathcal{T}$, only based on limited queries to the entries of the tensor \mathcal{T} . Let the cores of \mathcal{S} be denoted $\mathcal{A}_1, \dots, \mathcal{A}_d$.

In order to guarantee that $\tilde{q}_0 \approx \tilde{q}$, it suffices for the coefficient tensor to satisfy

$$\mathcal{B}[\mathcal{I}] \approx \langle \tilde{q}(\mathbf{x}), \phi_{\mathcal{I}}(\mathbf{x}) \rangle_{L^2(\Omega)}. \quad (3.11)$$

By replacing the integral on the right-hand side of (3.11) with numerical quadrature and replacing the values of \tilde{q} on the grid by the values furnished from the TT approximation \mathcal{S} , we can therefore construct \mathcal{B} as in Figure 3.3, where the weight matrix

$\mathbf{W} \in \mathbb{R}^{n \times m}$ is defined by

$$\mathbf{W}[i, j] = \phi_i(x^{(j)})w^{(j)}.$$

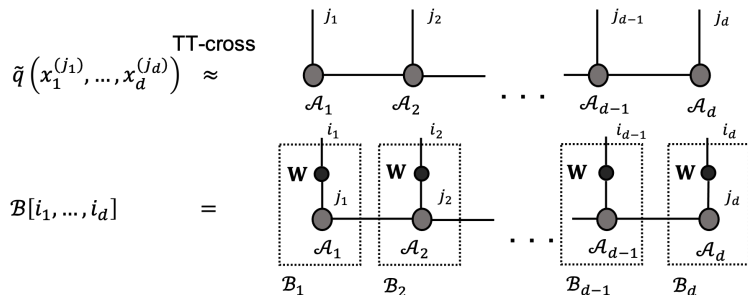


Fig. 3.3: Computing the TT of basis coefficients \mathcal{B} . (a) depicts our tensor train \mathcal{S} with cores $\mathcal{A}_1, \dots, \mathcal{A}_d$, approximating the tensor \mathcal{T} of the values of \tilde{q} on our multivariate grid. (b) shows how \mathcal{B} is constructed as a tensor train.

Finally we discuss how the properly normalized \mathcal{C} can be recovered from \mathcal{B} . Recalling that $p_0 = q_0^2$, where

$$q_0(\mathbf{x}) = \sum_{\mathcal{I}} \mathcal{C}[\mathcal{I}],$$

it can be seen readily using the orthonormality of the tensor product basis that

$$\int_{\Omega} p_0 d\mathbf{x} = \|q_0\|_{L^2(\Omega)} = \|\mathcal{C}\|_{\mathbb{F}} = \langle \mathcal{C}[\mathcal{I}], \mathcal{C}[\mathcal{I}] \rangle_{\mathcal{I}}.$$

In order to guarantee that our base distribution p_0 is in fact a normalized probability distribution, we therefore want to ensure $\|\mathcal{C}\|_{\mathbb{F}} = 1$.

In fact, $\|\mathcal{B}\|_{\mathbb{F}}$ can be computed by elementary TT contractions. Alternatively, if \mathcal{B} is put into right-left orthogonal form, then $\|\mathcal{B}\|_{\mathbb{F}}$ can be recovered as the Frobenius norm of only the first tensor core. Therefore we are motivated to define

$$\mathcal{C} = \frac{\mathcal{B}}{\|\mathcal{B}\|_{\mathbb{F}}}, \quad (3.12)$$

ensuring $\|\mathcal{C}\|_{\mathbb{F}} = 1$ as desired. The TT format for \mathcal{C} can be recovered from that of \mathcal{B} by rescaling only a single core, e.g., the first one (which would preserve right-left orthogonality, if \mathcal{B} is already put into right-left orthogonal form).

3.2. Flow model. Following Section 2.2, now that we have constructed a base distribution p_0 , it remains only to discuss the choice of flow model $F_{\theta}^{(k)}$, as well as how to optimize the loss (2.3)-(2.4).

In this work we use flows based on invertible residual networks, or iResNets [3, 6]. We choose the residual flow for its expressivity, as well as the convenience of initializing the flow map to be near the identity, as the base distribution may already offer a useful approximation of the target.

In the residual flow model, the flow maps are constructed as

$$F_{\boldsymbol{\theta}}^{(k)}(\mathbf{x}) = \mathbf{x} + G_{\boldsymbol{\theta}}^{(k)}(\mathbf{x}), \quad (3.13)$$

where the $G_{\boldsymbol{\theta}}^{(k)}$ are themselves parametrized by feed-forward neural networks. In variational inference, we do not need to invert $F_{\boldsymbol{\theta}}^{(k)}$ computationally, though invertibility is guaranteed if $G_{\boldsymbol{\theta}}^{(k)}$ is a contraction, and the Banach fixed point theorem enables efficient iterative computation of the inverse [32].

However, as mentioned in Section 2.2, it is important to be able to evaluate the Jacobian determinant of $F_{\boldsymbol{\theta}}^{(k)}$. This can be achieved by Taylor series expansion:

$$\log|DF_{\boldsymbol{\theta}}^{(k)}| = \log|I_d + DG_{\boldsymbol{\theta}}^{(k)}| = \text{Tr}(\log(I_d + DG_{\boldsymbol{\theta}}^{(k)})) = \sum_{m=1}^{\infty} (-1)^{m+1} \frac{\text{Tr}[(DG_{\boldsymbol{\theta}}^{(k)})^m]}{m}. \quad (3.14)$$

We can truncate the series (3.14) and use stochastic trace approximation via Hutchinson’s estimator [57] to accelerate the computation.

To accelerate training, we opted to add batch normalization [30] following each residual connection. Furthermore, since our base distribution is already rather close to the target distribution, we want to initialize the weights such that the map is near identity. To this end, all weights in the residual connection $g_{\boldsymbol{\theta}}$ are generated from a uniform distribution on $[-0.25, 0.25]$.

3.3. Summary. Here we summarize our proposed method for variational inference on the density $p(\mathbf{x}) \propto \exp(-U(\mathbf{x}))$, given the ability to evaluate the function $U(\mathbf{x})$.

1. Use TT-cross to construct a tensor train \mathcal{S} approximating the tensor \mathcal{T} (3.10) of values of $\tilde{q}(\mathbf{x}) := \exp(-U(\mathbf{x})/2)$ on our multivariate grid.
2. Via the construction of Figure 3.3 and (3.12), build a tensor train \mathcal{C} of basis coefficients, specifying $q_0(\mathbf{x})$ via (3.5). By construction, $p_0(\mathbf{x}) := q_0(\mathbf{x})^2$ is normalized and approximates the target $p(\mathbf{x})$.
3. Draw a corpus of samples $\mathbf{z}^{(1)}, \dots, \mathbf{z}^{(S)} \sim p_0$, equipped with densities $p_0(\mathbf{z}^{(s)})$, $s = 1, \dots, S$, following the algorithm described in Section 3.1.3.
4. Optimize the empirical loss (2.4), using the flow model specified in Section 3.2.

Further details of the training will be discussed in the Section 4 below, where numerical experiments are reviewed.

4. Numerical experiments. In this section, we demonstrate the ability of tensorizing flow to learn high-dimensional target distributions. We describe implementation details for constructing the TT base distribution in Section 4.1 and for flow training in Section 4.3. In Section 4.3, we present experiments on a Gaussian mixture distribution (Section 4.3.1), and Ginzburg-Landau models (Sections 4.3.2 and 4.3.3).

4.1. Details of base distribution construction. Recall that in our construction of the base distribution, we apply TT-cross to the tensor \mathcal{T} defined in (3.10) to obtain a tensor train \mathcal{S} . For our various experiments, we record in Table 4.1 the maximum TT rank of \mathcal{S} , which is also the maximum TT rank of the coefficient tensor \mathcal{C} . For benchmarking purposes, we also obtain a ground truth coefficient tensor $\mathcal{C}_{\text{true}}$ by specifying a local relative accuracy of 10^{-10} in TT-cross and allowing the ranks to be as large as needed to ensure this. These ranks are generally much higher than those of the low-rank approximations we use in our experiments and are also reported

in Table 4.1, along with the number n of univariate basis functions ϕ_1, \dots, ϕ_n , which we choose to be the Legendre polynomials.

Experiment	d	n	Max rank of $\mathcal{C}_{\text{true}}$	Max rank of \mathcal{C}
Gaussian mixture	30	512	116	2
1-D Ginzburg-Landau	25	50	30	2
2-D Ginzburg-Landau	64	30	694	3

Table 4.1: Details of base distribution construction for each experiment.

Computationally, we shift and scale all of our problems to the cube $[-1, 1]^d$, and we initialize the base distribution of all normalizing flows as $\mathcal{N}(0, 0.2I)$, chosen to ensure that all samples fall within the computational domain. In reporting our results, we shift and scale back to the original bounding box for the support of $p(\mathbf{x})$.

4.2. Details of flow model. We use a multi-layer perceptron (MLP) neural-network architecture with ReLU activations to define the residual connections in (3.13). The numbers of hidden layers (network depths) and layer widths used in our experiments are reported in Table 4.2. For training, we optimize with Adam [35], along with an exponential learning rate scheduler with a decay factor of 0.9999. We summarize the training hyperparameters in Table 4.3. As observed in [66], a smaller learning rate and larger batch size tend to yield stabler convergence of the model. To further stabilize the training, we implement gradient clipping such that the entries of the gradient always lie in the range $[-10^4, 10^4]$.

Experiment	Layer width	Network depth
Gaussian mixture	32	5
1-D Ginzburg-Landau	32	5
2-D Ginzburg-Landau	64	5

Table 4.2: Neural network widths and depths.

Experiment	Batch size	Learning rate	Number of epochs	Flow length
Gaussian mixture	128	5×10^{-4}	200	10
1-D Ginzburg-Landau	256	5×10^{-4}	200	12
2-D Ginzburg-Landau	64	3×10^{-5}	200	12

Table 4.3: Training hyperparameters.

For consistency, we compare the performance of TF and NF under the exact same training conditions. All flow models are trained using a training set of size $S_{\text{train}} = 10^4$ and validated on a holdout set of size $S_{\text{holdout}} = 10^4$. For both TF and NF, we will plot the loss (2.4) evaluated using the holdout samples. The validation loss will be reported as an average over 10 training runs with random network initializations.

4.3. Examples. Here we apply the tensorizing flow and compare its performance with traditional normalizing flow on a range of high-dimensional densities.

To quantify the performance of TF relative to that of NF, we define $-\log Z_{\text{true}}$ to be the loss (2.4) estimated from a very high-fidelity tensor train, obtained as described in Section 4.1. Likewise we define $-\log Z_{\text{TF}}$ and $-\log Z_{\text{NF}}$ to be the final losses after training of the tensorizing and normalizing flows, respectively. Then we define the

error ratio:

$$\text{Error Ratio} := \frac{\log Z_{\text{true}} - \log Z_{\text{TF}}}{\log Z_{\text{true}} - \log Z_{\text{NF}}}. \quad (4.1)$$

Note that both the numerator and denominator must be positive.

4.3.1. Gaussian mixture model. First we consider a synthetic example in dimension $d = 30$, defined as a mixture of five Gaussians. The means are: $\boldsymbol{\mu}^{(1)} = [0, \dots, 0, 2, 2]^\top$, $\boldsymbol{\mu}^{(2)} = [0, \dots, 0, 2, -2]^\top$, $\boldsymbol{\mu}^{(3)} = [0, \dots, 0, -2, 2]^\top$, $\boldsymbol{\mu}^{(4)} = [0, \dots, 0, -2, -2]^\top$, and $\boldsymbol{\mu}^{(5)} = [0, \dots, 0, 0, 0]^\top$. Then we define matrices $\boldsymbol{\Sigma}^{(i)}$, $i = 1, \dots, 5$ as the identity, except in the 2×2 block corresponding to the last two dimensions, where we take:

$$\boldsymbol{\Sigma}_{d-1:d, d-1:d}^{(1)} = \boldsymbol{\Sigma}_{d-1:d, d-1:d}^{(4)} = \begin{bmatrix} 1 & 19/20 \\ 19/20 & 1 \end{bmatrix}$$

and

$$\boldsymbol{\Sigma}_{d-1:d, d-1:d}^{(2)} = \boldsymbol{\Sigma}_{d-1:d, d-1:d}^{(3)} = \begin{bmatrix} 1 & -19/20 \\ -19/20 & 1 \end{bmatrix}.$$

Then we define a $p(\mathbf{x})$ as the equally weighted mixture of the Gaussian distributions $\mathcal{N}(\boldsymbol{\mu}^{(i)}, 0.4 \times \boldsymbol{\Sigma}^{(i)})$, $i = 1, \dots, 5$.

Figures 4.1 (a) and (d) depict various marginals of p , demonstrating multimodality clearly. Figure 4.1 (b), (c), (e), and (f) depict marginal density estimates produced from the trained NF and TF.

For comparison, corresponding marginal density estimates produced from the TT base distribution p_0 are presented in Figure 4.2.

We can see that the TF is more capable of capturing multimodality of the target, even given a base distribution that is very coarse, involving only a TT of rank 2, which is the minimal nontrivial rank. Meanwhile the NF fails to capture the modes with a unimodal base distribution. We quantitatively confirm the effectiveness of TF in the validation loss plot of Figure 4.3 and Table 4.4.

Base distribution	Start	End	$-\log Z_{\text{true}}$	Error Ratio
TT (rank 2)	21.5266	20.1952	<u>20.1794</u>	<u>0.0271</u>
Gaussian	33.4478	20.7634		

Table 4.4: Training synopsis for TF and NF applied to the Gaussian mixture model.

4.3.2. One-dimensional Ginzburg-Landau model. Ginzburg-Landau theory offers a variety of nontrivial sampling problems relevant to the study of phase transitions and rare events [28]. Traditional sampling methods are often inadequate even for simple models [46]. In this section, we consider a Ginzburg-Landau-type model for an antiferromagnet on a 1D lattice, where the states of neighboring sites prefer to orient oppositely. More precisely, we denote the states at $(d + 2)$ lattice points as $u_0, u_1, \dots, u_{d+1} \in \mathbb{R}$, subject to the boundary conditions $u_0 = u_{d+1} = 0$. The energy function is defined as follows:

$$E(u_1, \dots, u_d) := - \sum_{i=1}^{d+1} \frac{\delta}{2} \left(\frac{u_i - u_{i-1}}{h} \right)^2 + \frac{1}{4\delta} \sum_{i=1}^d (1 - u_i^2)^2, \quad (4.2)$$

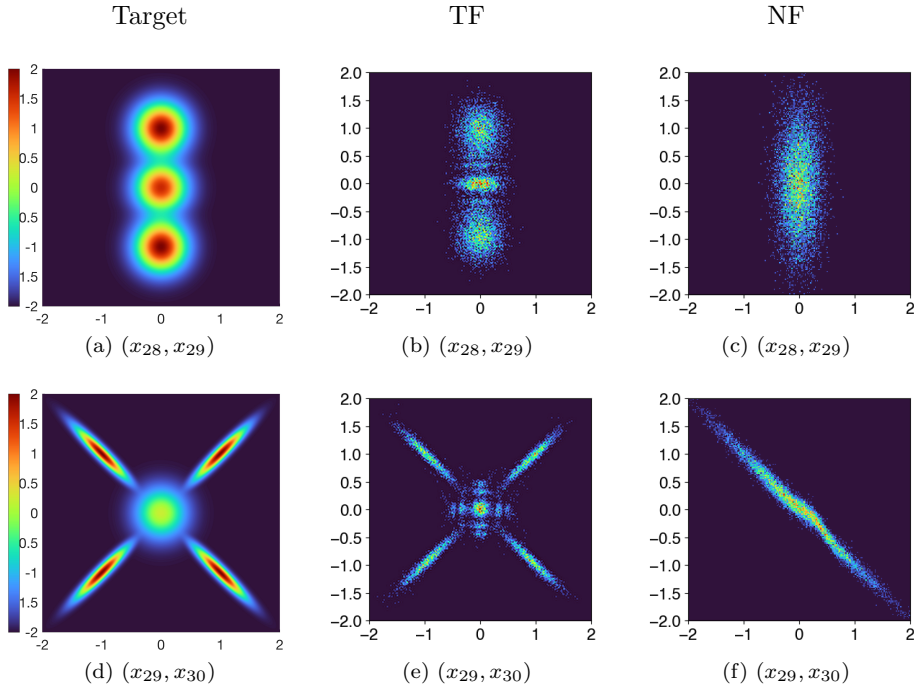


Fig. 4.1: Marginals of the Gaussian mixture model corresponding to variables (x_{28}, x_{29}) and (x_{29}, x_{30}) . (a)(d): Ground truth marginal densities. (b)(e): Marginal density estimates obtained from sampling the trained TF. (c)(f): Marginal density estimates obtained from sampling the trained NF.

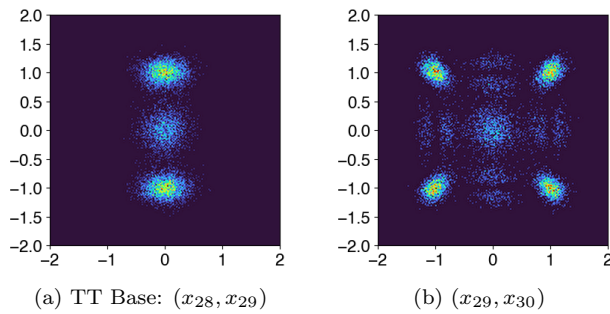


Fig. 4.2: Estimated marginals of the Gaussian mixture model obtained directly from the rank-2 tensor train base distribution p_0 , without flow.

where $\delta > 0$ is a scalar parameter and $h > 0$ is the lattice spacing. The final term in (4.2) is a double-well potential ensuring (when δ is small) that the u_i take values near ± 1 . The target probability density is then defined

$$p(\mathbf{u}) \propto \exp(-\beta E(\mathbf{u})), \quad (4.3)$$

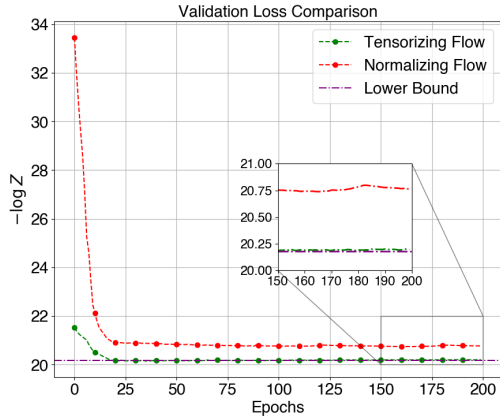


Fig. 4.3: Validation loss plot for TF and NF over the course of training for the Gaussian mixture distribution.

where β is the inverse temperature. The energy function has two minimizers, yielding a bimodal distribution.

In our experiment, we set $d = 35$, $h = 1/(d + 1) = 1/36$, $\beta = 6.25 \times 10^{-2}$, and $\delta = 0.04$. We visualize one typical representative of each mode (drawn from p_{true}) in Figure 4.4.

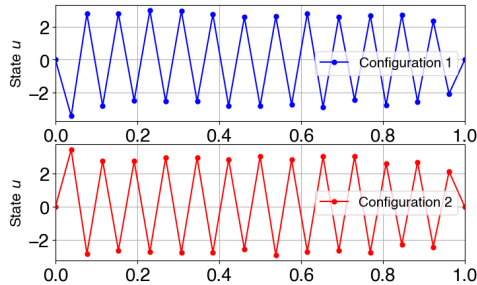


Fig. 4.4: One typical sample configuration from each mode of (4.3).

Typical sample configurations generated by the TF and NF, before and after training, are plotted in Figures 4.5 and 4.6, respectively. We observe that the trained NF samples sometimes appear to be qualitatively incorrect, and the improvement of TF over NF is confirmed quantitatively in terms of the validation loss, as summarized in Table 4.5 and plotted in Figure 4.7.

Base Distribution	Start	End	$-\log Z_{\text{true}}$	Error Ratio
TT (rank 2)	222.736	-202.756		
Gaussian	551.411	-172.069	<u>-208.014</u>	<u>0.146</u>

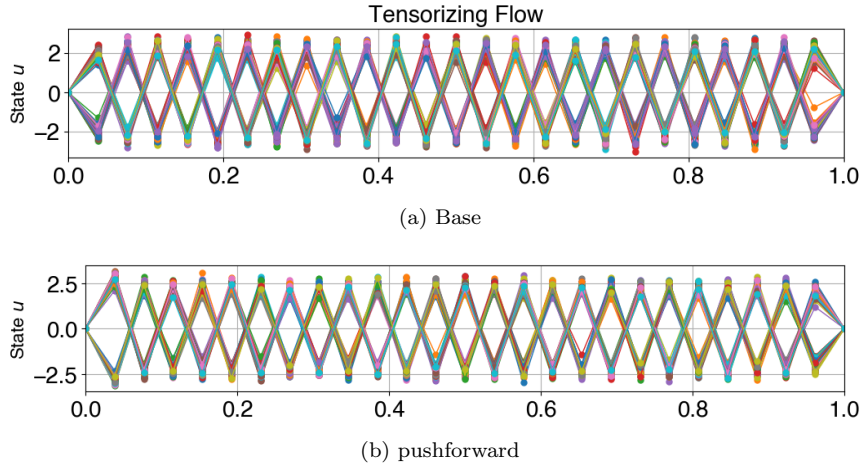


Fig. 4.5: Several typical sample configurations of the 1-dimensional Ginzburg-Landau model drawn from the TF (a) before training and (b) after training.

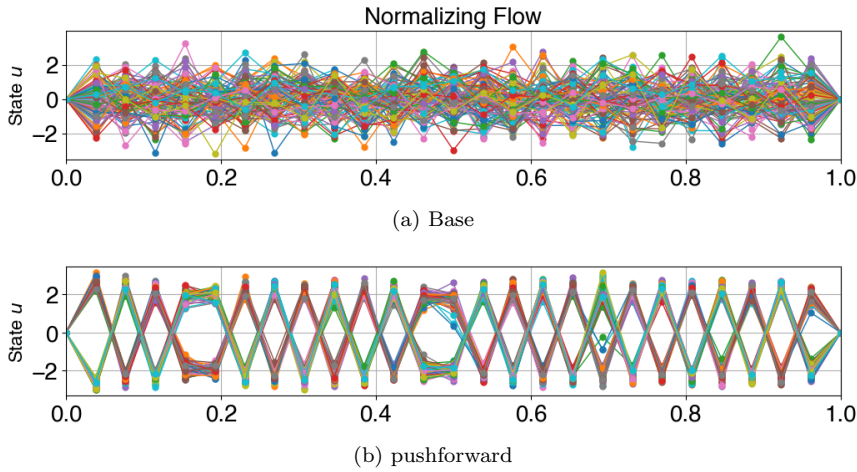


Fig. 4.6: Several typical sample configurations of the 1-dimensional Ginzburg-Landau model drawn from the NF (a) before training and (b) after training.

Table 4.5: Training synopsis for TF and NF applied to the 1-dimensional Ginzburg-Landau model.

4.3.3. Two-Dimensional Ginzburg-Landau model. In this section, we consider an analogous Ginzburg-Landau-type model on a two-dimensional, $(d + 2) \times (d + 2)$ square lattice. We denote the values of the scalar field at lattice points as $u_{i,j}$,

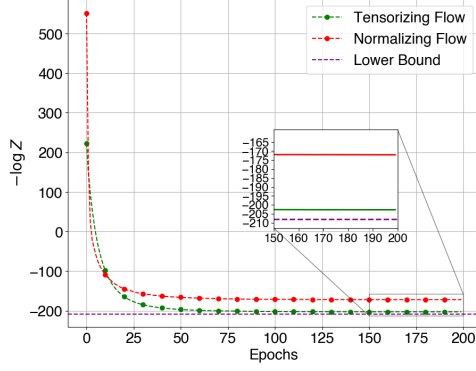


Fig. 4.7: Validation loss plot for TF and NF over the course of training for the 1-dimensional Ginzburg-Landau model.

$i, j = 0, \dots, d + 1$, and define the energy:

$$E(\mathbf{u}) := \frac{\delta}{2} \left[\sum_{i=1}^{d+1} \sum_{j=1}^{d+1} \left(\frac{u_{i,j} - u_{i-1,j}}{h} \right)^2 + \left(\frac{u_{i,j} - u_{i,j-1}}{h} \right)^2 \right] + \frac{1}{4\delta} \sum_{i=1}^d \sum_{j=1}^d (1 - u_{i,j}^2)^2, \quad (4.4)$$

with boundary conditions

$$u_{0,:} = u_{d+1,:} = \mathbf{1}, \quad u_{:,0} = u_{:,d} = -\mathbf{1}. \quad (4.5)$$

Once again $\delta > 0$ is a scalar parameter, and $h > 0$ is the lattice spacing. The target distribution is again defined by

$$p(\mathbf{u}) \propto \exp(-\beta E(\mathbf{u})). \quad (4.6)$$

We set $d = 64$, $h = 1/(d + 1) = 1/9$, $\beta = 0.2$, and $\delta = 0.04$.

Typical sample configurations generated by the trained TF and NF are plotted in Figure 4.8. Qualitative differences are visually apparent.

In Figure 4.9, we plot empirical estimates for:

$$\bar{u}_{i,j} := \mathbb{E}[u_{i,j}] \quad (4.7)$$

obtained from $S = 2 \times 10^4$ samples from both the TF and NF, as well as the reference p_{true} , which we denote respectively as \bar{u}_{TF} , \bar{u}_{NF} , and \bar{u}_{true} . In Figure 4.10, we plot the absolute errors of \bar{u}_{TF} and \bar{u}_{NF} , demonstrating the advantage of TF more clearly.

The improvement of TF over NF is again confirmed quantitatively via the validation loss, plotted in Figure 4.11 and summarized in Table 4.6.

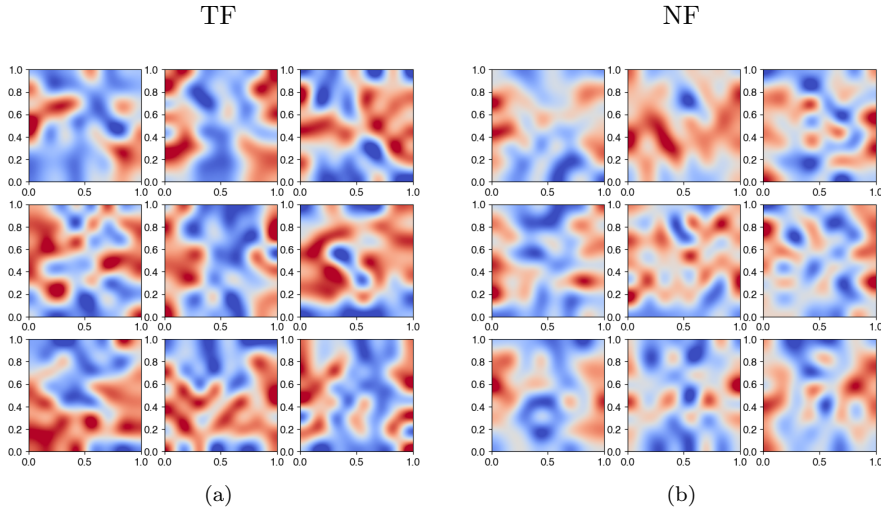


Fig. 4.8: Several typical sample configurations of the 2-dimensional Ginzburg-Landau model drawn from (a) the trained TF and (b) the trained NF.

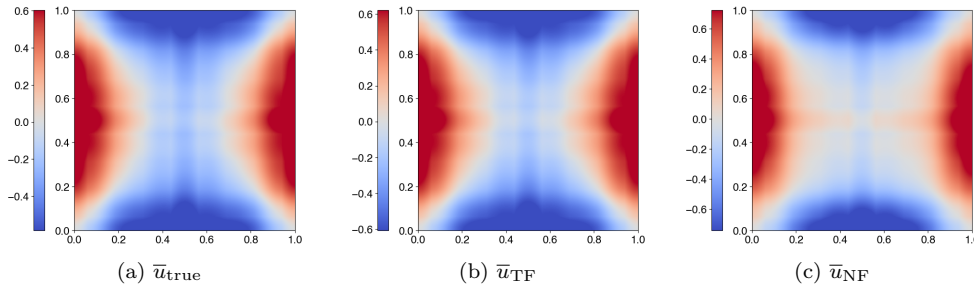


Fig. 4.9: GL 2-Dim: Estimated first moment of sampled states \bar{u} defined in (4.7). (a) Ground truth (b) TF (c) NF. All \bar{u}_{true} , \bar{u}_{TF} , and \bar{u}_{NF} are computed with $S = 20000$ samples.

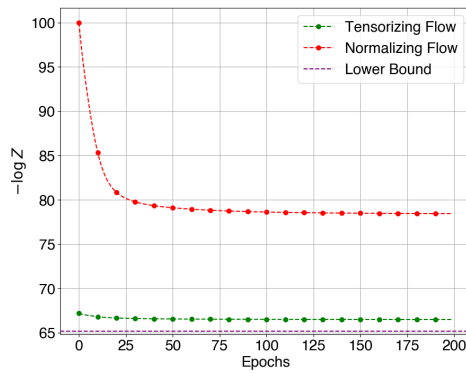


Fig. 4.11: Validation loss plot for TF and NF over the course of training for the 2-dimensional Ginzburg-Landau model.

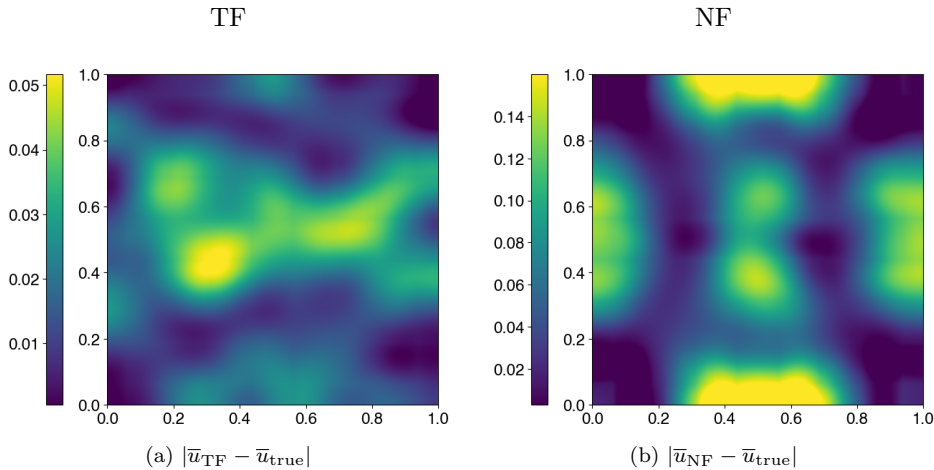


Fig. 4.10: GL 2-Dim: (a) Pointwise absolute errors between \bar{u}_{TF} and \bar{u}_{true} , defined in (4.7). (b) Pointwise absolute errors between \bar{u}_{NF} and \bar{u}_{true} , defined in (4.7). Errors are plotted with respect to each lattice point (i, j) in $[0, 1]^2$.

Base Distribution	Start	End	$-\log Z_{\text{true}}$	Error Ratio
Rank 3 TT	67.202	66.488	<u>65.198</u>	<u>0.0974</u>
$\mathcal{N}(\mathbf{0}, 0.2\mathbf{I}_{64})$	99.979	78.438		

Table 4.6: Training synopsis for TF and NF applied to the 2-dimensional Ginzburg-Landua model.

5. Conclusion. In this paper, we propose a flexible ansatz for variational inference, *tensorizing-flow*, by combining a neural-network flow model with a low rank TT base distribution. Such a base distribution can be obtained via numerical linear algebra routines and captures non-trivial overlaps with the target distribution. The representation power of the neural-network flow model then serves to bridge the approximation gap. Finally, effectiveness of the TT base measure is concretized by tighter variational lower bound convergence in several high-dimensional examples.

REFERENCES

- [1] M. S. ALBERGO, G. KANWAR, AND P. E. SHANAHAN, *Flow-based generative models for markov chain monte carlo in lattice field theory*, Physical Review D, 100 (2019).
- [2] MICHAEL S. ALBERGO AND ERIC VANDEN-EIJNDEN, *Building normalizing flows with stochastic interpolants*, 2022.
- [3] JENS BEHRMANN, WILL GRATHWOHL, RICKY T. Q. CHEN, DAVID DUVENAUD, AND JÖRN-HENRIK JACOBSEN, *Invertible residual networks*, (2018).
- [4] DAVID M. BLEI, ALP KUCUKELBIR, AND JON D. MCAULIFFE, *Variational inference: A review for statisticians*, Journal of the American Statistical Association, 112 (2017), pp. 859–877.
- [5] JACOB C BRIDGEMAN AND CHRISTOPHER T CHUBB, *Hand-waving and interpretive dance: an introductory course on tensor networks*, Journal of Physics A: Mathematical and Theoretical, 50 (2017), p. 223001.
- [6] RICKY T. Q. CHEN, JENS BEHRMANN, DAVID DUVENAUD, AND JÖRN-HENRIK JACOBSEN, *Residual flows for invertible generative modeling*, 2019.

- [7] RICKY T. Q. CHEN, YULIA RUBANOVA, JESSE BETTENCOURT, AND DAVID DUVENAUD, *Neural ordinary differential equations*, 2018.
- [8] ANDRZEJ CICHOCKI, NAMGIL LEE, IVAN OSELEDETS, ANH-HUY PHAN, QIBIN ZHAO, AND DANILO P. MANDIC, *Tensor networks for dimensionality reduction and large-scale optimization: Part 1 low-rank tensor decompositions*, Foundations and Trends® in Machine Learning, 9 (2016), pp. 249–429.
- [9] BRIAN COYLE, DANIEL MILLS, VINCENT DANOS, AND ELHAM KASHEFI, *The born supremacy: quantum advantage and training of an ising born machine*, npj Quantum Information, 6 (2020), p. 60.
- [10] TIANGANG CUI AND SERGEY DOLGOV, *Deep composition of tensor-trains using squared inverse rosenblatt transports*, Foundations of Computational Mathematics, (2021).
- [11] ———, *Deep composition of tensor-trains using squared inverse rosenblatt transports*, Foundations of Computational Mathematics, (2021).
- [12] M. NAZARETH DA COSTA, R. ATTUX, A. CICHOCKI, AND J. M. T. ROMANO, *Tensor-train networks for learning predictive modeling of multidimensional data*, 2021.
- [13] HUSSAM AL DAAS, GREY BALLARD, AND PETER BENNER, *Parallel algorithms for tensor train arithmetic*, 2020.
- [14] LIEVEN DE LATHAUWER, BART DE MOOR, AND JOOS VANDEWALLE, *A multilinear singular value decomposition*, SIAM Journal on Matrix Analysis and Applications, 21 (2000), pp. 1253–1278.
- [15] LAURENT DINH, DAVID KRUEGER, AND YOSHUA BENGIO, *Nice: Non-linear independent components estimation*, 2014.
- [16] LAURENT DINH, JASCHA SOHL-DICKSTEIN, AND SAMY BENGIO, *Density estimation using real nvp*, 2016.
- [17] SERGEY DOLGOV, KARIM ANAYA-IZQUIERDO, COLIN FOX, AND ROBERT SCHEICHL, *Approximation and sampling of multivariate probability distributions in the tensor train decomposition*, 2018.
- [18] MATTHEW FELLOWS, ANUJ MAHAJAN, TIM G. J. RUDNER, AND SHIMON WHITESON, *Virel: A variational inference framework for reinforcement learning*, 2018.
- [19] MARYLOU GABRIÉ, GRANT M. ROTSKOFF, AND ERIC VANDEN-EIJNDEN, *Efficient bayesian sampling using normalizing flows to assist markov chain monte carlo methods*, arXiv:2107.08001.
- [20] MARYLOU GABRIÉ, GRANT M. ROTSKOFF, AND ERIC VANDEN-EIJNDEN, *Adaptive monte carlo augmented with normalizing flows*, Proceedings of the National Academy of Sciences, 119 (2022).
- [21] PATRICK GELSS, *The Tensor-Train Format and Its Applications*, PhD thesis, 2017.
- [22] SAMUEL GERSHMAN, MATT HOFFMAN, AND DAVID BLEI, *Nonparametric variational inference*, 2012.
- [23] IAN J. GOODFELLOW, JEAN POUGET-ABADIE, MEHDI MIRZA, BING XU, DAVID WARDE-FARLEY, SHERJIL OZAIR, AARON COURVILLE, AND YOSHUA BENGIO, *Generative adversarial networks*, 2014.
- [24] WILL GRATHWOHL, RICKY T. Q. CHEN, JESSE BETTENCOURT, ILYA SUTSKEVER, AND DAVID DUVENAUD, *Fjord: Free-form continuous dynamics for scalable reversible generative models*, 2018.
- [25] JESPER L. HINRICH AND MORTEN MØRUP, *Probabilistic tensor train decomposition*, in 2019 27th European Signal Processing Conference (EUSIPCO), 2019, pp. 1–5.
- [26] P.C. HOHENBERG AND A.P. KREKHOV, *An introduction to the ginzburg–landau theory of phase transitions and nonequilibrium patterns*, Physics Reports, 572 (2015), pp. 1–42.
- [27] SEBASTIAN HOLTZ, THORSTEN ROHWEDDER, AND REINHOLD SCHNEIDER, *The alternating linear scheme for tensor optimization in the tensor train format*, SIAM Journal on Scientific Computing, 34 (2012), pp. A683–A713.
- [28] RUDOLF PETER HUEBENER, *Ginzburg-Landau Theory*, Springer Berlin Heidelberg, Berlin, Heidelberg, 1979, pp. 33–57.
- [29] YH. HUR, J. G. HOSKINS, M. LINDSEY, E. M. SToudenMIRE, AND Y. KHOO, *Generative modeling via tensor train sketching*, 2022.
- [30] SERGEY IOFFE AND CHRISTIAN SZEGEDY, *Batch normalization: Accelerating deep network training by reducing internal covariate shift*, 2015.
- [31] PRIYANK JAINI, IVAN KOBYZEV, YAOLIANG YU, AND MARCUS BRUBAKER, *Tails of lipschitz triangular flows*, 2019.
- [32] C.A. JENSEN, R.D. REED, R.J. MARKS, M.A. EL-SHARKAWI, JAE-BYUNG JUNG, R.T. MIYAMOTO, G.M. ANDERSON, AND C.J. EGGEN, *Inversion of feedforward neural networks: algorithms and applications*, Proceedings of the IEEE, 87 (1999), pp. 1536–1549.

- [33] MICHAEL I. JORDAN, ZUBIN GHAHRAMANI, TOMMI S. JAAKKOLA, AND LAWRENCE K. SAUL, *An introduction to variational methods for graphical models*, Machine Learning, 37 (1999), pp. 183–233.
- [34] BORIS N. KHOROMSKIY AND CHRISTOPH SCHWAB, *Tensor-structured galerkin approximation of parametric and stochastic elliptic pdes*, SIAM Journal on Scientific Computing, 33 (2011), pp. 364–385.
- [35] DIEDERIK P. KINGMA AND JIMMY BA, *Adam: A method for stochastic optimization*, 2014.
- [36] DIEDERIK P. KINGMA AND PRAFULLA DHARIWAL, *Glow: Generative flow with invertible 1x1 convolutions*, 2018.
- [37] DURK P KINGMA, SHAKIR MOHAMED, DANILO JIMENEZ REZENDE, AND MAX WELLING, *Semi-supervised learning with deep generative models*, in Advances in Neural Information Processing Systems, Z. Ghahramani, M. Welling, C. Cortes, N. Lawrence, and K.Q. Weinberger, eds., vol. 27, Curran Associates, Inc., 2014.
- [38] DIEDERIK P KINGMA AND MAX WELLING, *Auto-encoding variational bayes*, 2013.
- [39] ILYA KISIL, GIUSEPPE G. CALVI, KRITON KONSTANTINIDIS, YAO LEI XU, AND DANILO P. MANDIC, *Reducing computational complexity of tensor contractions via tensor-train networks*, 2021.
- [40] STEFAN KLUS, PATRICK GELSS, SEBASTIAN PEITZ, AND CHRISTOF SCHÜTTE, *Tensor-based dynamic mode decomposition*, Nonlinearity, 31 (2018), pp. 3359–3380.
- [41] IVAN KOBYZEV, SIMON J.D. PRINCE, AND MARCUS A. BRUBAKER, *Normalizing flows: An introduction and review of current methods*, IEEE Transactions on Pattern Analysis and Machine Intelligence, 43 (2021), pp. 3964–3979.
- [42] TAMARA G. KOLDA AND BRETT W. BADER, *Tensor decompositions and applications*, SIAM Review, 51 (2009), pp. 455–500.
- [43] ALEJANDRO LAGE-CASTELLANOS, ROBERTO MULET, FEDERICO RICCI-TERSENGHI, AND TOMMASO RIZZO, *Inference algorithm for finite-dimensional spin glasses: Belief propagation on the dual lattice*, Phys. Rev. E, 84 (2011), p. 046706.
- [44] MIKE LASZKIEWICZ, JOHANNES LEDERER, AND ASJA FISCHER, *Copula-based normalizing flows*, 2021.
- [45] QIANXIAO LI, BO LIN, AND WEIQING REN, *Computing committor functions for the study of rare events using deep learning*, The Journal of Chemical Physics, 151 (2019), p. 054112.
- [46] QIANXIAO LI, BO LIN, AND WEIQING REN, *Computing committor functions for the study of rare events using deep learning*, The Journal of Chemical Physics, 151 (2019), p. 054112.
- [47] ANDRIY MNH AND KAROL GREGOR, *Neural variational inference and learning in belief networks*, (2014).
- [48] GEORGII S. NOVIKOV, MAXIM E. PANOV, AND IVAN V. OSELEDETS, *Tensor-train density estimation*, in Proceedings of the Thirty-Seventh Conference on Uncertainty in Artificial Intelligence, Cassio de Campos and Marloes H. Maathuis, eds., vol. 161 of Proceedings of Machine Learning Research, PMLR, 27–30 Jul 2021, pp. 1321–1331.
- [49] FRANK NOÉ, SIMON OLSSON, JONAS KÖHLER, AND HAO WU, *Boltzmann generators: Sampling equilibrium states of many-body systems with deep learning*, Science, 365 (2019), p. eaaw1147.
- [50] ROMÁN ORÚS, *A practical introduction to tensor networks: Matrix product states and projected entangled pair states*, Annals of Physics, 349 (2014), pp. 117–158.
- [51] IVAN OSELEDETS AND EUGENE TYRTYSHNIKOV, *Tt-cross approximation for multidimensional arrays*, Linear Algebra and its Applications, 432 (2010), pp. 70–88.
- [52] I. V. OSELEDETS, *Tensor-train decomposition*, SIAM Journal on Scientific Computing, 33 (2011), pp. 2295–2317.
- [53] G. PAPAMAKARIOS, E. NALISNICK, D. REZENDE, S. MOHAMED, AND B. LAKSHMINARAYANAN, *Normalizing flows for probabilistic modeling and inference*, J. Mach. Learn. Res., 22 (2021), pp. 1–64.
- [54] D. REZENDE AND S. MOHAMED, *Variational inference with normalizing flows*, in ICML, 2015.
- [55] ABRAM RODGERS AND DANIELE VENTURI, *Implicit step-truncation integration of nonlinear pdes on low-rank tensor manifolds*, 2022.
- [56] TIANYI SHI, MAXIMILIAN RUTH, AND ALEX TOWNSEND, *Parallel algorithms for computing the tensor-train decomposition*, 2021.
- [57] MACIEJ SKORSKI, *Modern analysis of hutchinson’s trace estimator*, in 2021 55th Annual Conference on Information Sciences and Systems (CISS), 2021, pp. 1–5.
- [58] MICHELINE B. SOLEY, PAUL BERGOLD, ALEX A. GORODETSKY, AND VICTOR S. BATISTA, *Functional tensor-train chebyshev method for multidimensional quantum dynamics simulations*, Journal of Chemical Theory and Computation, 18 (2021), pp. 25–36.
- [59] JOSHUA S. SPEAGLE, *A conceptual introduction to markov chain monte carlo methods*, 2019.

- [60] VINCENT STIMPER, BERNHARD SCHÖLKOPF, AND JOSÉ MIGUEL HERNÁNDEZ-LOBATO, *Resampling base distributions of normalizing flows*, (2021).
- [61] E. MILES STOUDENMIRE AND DAVID J. SCHWAB, *Supervised learning with quantum-inspired tensor networks*, (2016).
- [62] E. G. TABAK AND C. V. TURNER, *A family of nonparametric density estimation algorithms*, *Comm. Pure Appl. Math.*, 66 (2013), p. 145.
- [63] E. G. TABAK AND E. VANDEN-ELJNDEN, *Density estimation by dual ascent of the log-likelihood*, *Comm. Math. Sci.*, 8 (2010), p. 217.
- [64] ROBERT TEMPKE AND TERENCE MUSHO, *Autonomous design of new chemical reactions using a variational autoencoder*, *Communications Chemistry*, 5 (2022), p. 40.
- [65] MICHALIS K. TITSIAS, *Learning model reparametrizations: Implicit variational inference by fitting mcmc distributions*, 2017.
- [66] YU WANG, FANG LIU, AND DANIELE E. SCHIAVAZZI, *Variational inference with nofas: Normalizing flow with adaptive surrogate for computationally expensive models*, 2021.
- [67] STEVEN R. WHITE, *Density-matrix algorithms for quantum renormalization groups*, *Phys. Rev. B*, 48 (1993), pp. 10345–10356.
- [68] MIKE WU, KRISTY CHOI, NOAH GOODMAN, AND STEFANO ERMON, *Meta-amortized variational inference and learning*, 2019.
- [69] LE XU, LEI CHENG, NGAI WONG, AND YIK-CHUNG WU, *Tensor train factorization and completion under noisy data with prior analysis and rank estimation*, 2020.